MTLA 40 (2025) 102391

Contents lists available at ScienceDirect

Materialia

journal homepage: www.elsevier.com/locate/mtla

Full length article

Grain growth simulation of steels during heat treatment with statistically modeled discrete neighborhood

Marc Laub [a,*], Eric Detemple [b], Sebastian Scholl [b], Christian Motz [a]

[a] Saarland University, Chair for Material Science and Methods, Saarbuecken, 66123, Saarland, Germany
[b] AG der Dillinger Hüttenwerke, Dillingen/Saar, 66763, Saarland, Germany

ARTICLE INFO

Keywords:
Simulation
Grain growth
Microstructure
Austenite
Discrete neighborhood
Statistical

ABSTRACT

A new grain growth model is proposed that extends classical mean-field models to include the local neighborhood of grains. The theoretical basis of the approach is the equilibrium angle of grain boundaries at triple junctions, which is estimated to be 120° considering 2 dimensions, in the case of isotropic grain boundary energy. Based on this fact and a size comparison of individual grains, an algorithm is developed that assigns a discrete neighborhood relationship to all grains, resulting in the generation of an artificial microstructure. For validation, samples of a CMn steel were examined in different states after heat treatments and the microstructure was characterized using deep learning approaches to extract grain boundaries from etched samples with excellent statistics and reliability. The properties and statistical characteristics of the artificial and real microstructures are presented and compared. It is shown that simple topological approaches, such as the linear relationship between the number of grain neighbors and the relative grain size, are good only in a first approximation, but collapse in detail. The proposed model is able to resemble these small deviations of a real microstructure from topological models. Furthermore, the grain growth behavior of such an artificial microstructure is compared with real grain growth experiments. The comparison shows that by implementing the discrete neighborhood of grains, behaviors such as abnormal grain growth seem to be covered to a certain extent without additional treatment as required in other models.

1. Introduction

The manipulation of grain growth in such a way, that microstructural dependent properties evolve favorable, is the high art of thermomechanical processing of steel slabs toward the ready for sale products. Properties as the yield strength or the velocity of the recrystallization kinetic are directly connected to the grain size by the Hall–Patch effect. Depending on how exact those properties have to be adjusted, the time slots of the necessary processing steps need to be hit to the second. Hence knowledge about the microstructure is a huge benefit.

Grain growth simulations have over time become the tool of choice when it comes to predict the evolution of microstructure, but these forecasts are only as good as the included physics. If grain size refining mechanisms such as recrystallization are neglected, the grain size distribution during grain growth is inalterable over time if the examined histogram is normed on the mean grain size [1]. The distribution itself can be described by a logarithmic normal distribution [2]. This basic rule can simply be illustrated by a Voronoi tessellation, where the seeds are not put in place at the same time but one after another, resulting in a power-diagram or Laguerre–Voronoi diagram. The rate of microstructural evolution slows down as it evolves toward an asymptotic state [3]. A grain growth simulation should be able to cover all these features. One of the earliest models for grain size prediction was proposed by Burke [4], suggesting that the driving force of a grain boundary to move is proportional to its curvature and its direction is toward its center of curvature. This fact is often represented as an inverse proportionality of the grains diameter as the corresponding curvature, that originally results from the reduction of interfacial energy as stated by [5–7].

This model described the microstructure evolution with only few parameters, depending on the (initial) grain size, time passed during heat treatment and proportional constants [4], but over time, more advanced models arose, more and more focusing on local events that required simulations capable to circumstantiate grain boundary movement with lateral resolution. Phase field models [8], cellular automata models [9], Monte Carlo Potts models [10,11] and vertex models [12] are the most popular modern frameworks. They all have their advantages and disadvantages, just to name the compact data in vertex models or the continuum descriptions in phase field models on the

* Corresponding author.
E-mail address: m.laub@matsci.uni-saarland.de (M. Laub).

https://doi.org/10.1016/j.mtla.2025.102391
Received 9 September 2024; Accepted 12 March 2025
Available online 22 March 2025

positive side, but also the required discretization of space that is a major drawback for all of them since the discretization limits the fidelity of the simulation, as noted by [13]. In the same work, [13] provides a solution for the space discretization problem in two dimensions by presenting a model, that based on the assumptions of [14] calculates the movement of triple junctions and boundary vertices without the necessity of discretization. It can easily be expanded to three dimensions as demonstrated in [15,16]. Although this model permits a very sophisticated way to calculate the movement of grain boundaries at discrete time steps, vertex models lack a fundamental feature. The fact, that grains itself do not exist in vertex models, but are only defined by the boundaries that limit their spatial distention, makes it hard to implement additional driving forces that result from characteristics of the grain itself, contrary to the forces yielding from the curvature of the boundary. Such properties, namely the dislocation density, cannot be neglected when it comes to strain induced grain growth or recrystallization, two peculiarities that are impossible to circumnavigate during hot forming.

Also the validation of a grain growth model is important. This task is often not trivial, since the grain size of the high temperature phase has to be determined. While [17] overcame this problem by measuring the grain size insitu via laser ultrasound, this method might not be applicable for the vast majority of users. Notwithstanding this method provides an excellent time resolution, only providing a mean value, this methods is unfeasible if the shape of the grain size distribution is of interest. In such cases more direct methods should be considered such as the reconstruction of the prior austenitic phase from EBSD orientation data which is applicable for martensitic and partially bainitic structures after quenching [18] or the conventional etching of the specimens with the standard Bechet–Beaujard-etchand [19] or with modified recipes [20]. For extreme low carbon steels the choice of the wetting agent as stated by [21] has a large impact on the results as can be seen in [22]. For the sake of completeness thermal etching can also be named in this context and can be gathered in [23].

2. Mean field models

In many cases, not only the capability of the model is of interest, but also the time required by the simulation itself. If no detailed lateral information about the microstructure is of interest, a more inchoate model, that still provides the desired quantities, might be the better choice. Most of these models are still focused on the mean grain boundary curvature, based on the work of [4,24] or on the number of sides (coordination number) of the grains, as shown by [25,26]. These early models illustrate the meaning of mean-field models, by reducing the microstructure in all its facettes to a only one parameter, the mean grain size, as can be seen in Eq. (1) of the Burke–Turnbull model.

$$\frac{d\overline{R}}{dt} \propto \frac{\gamma_{GB}}{\overline{R}} \tag{1}$$

Here γ_{GB} is the isotropic grain boundary energy and $\overline{R}$ the mean grain size.

Hillert [3] for example considered individual grains R_i that are surrounded by a hypothetical medium, that represents the average microstructure by the mean grain size $\overline{R}$, thus altering the Burke–Turnbull model. The advantage of this model is, that the result is not only a mean grain size, but a full grain size distribution, which contains much more information.

$$\frac{d\overline{R}}{dt} \propto \gamma_{GB}\left(\frac{1}{\overline{R}} - \frac{1}{R_i}\right) \tag{2}$$

Later, [27] further improved Hillert's model. He argued that Hillert's assumption of $\overline{R}$ representing the average microstructure, is only true if the system is large enough. For smaller systems, or more localized observations, $\overline{R}$ should show variations. A grain of particular size could therefore shrink in one place, but grow at another. These local variations of grain growth are not covered by Hillert. The constant growth rate provided by Eq. (2) are therefore only valid after a stationary grain size distribution is already obtained, thus only describing normal grain growth. By assigning individual neighboring grains to each single grain, [27] bypassed this problem with his so called linear bubble model. The assignment of the neighborhood for his 1 dimensional growth scenario is given by:

$$4\pi\ (R_i + \overline{R})^2 = \sum_{j=1}^{j_{max}} \pi\ min(R_i^2, R_j^2) \tag{3}$$

This equation basically tries to occupy the surface of a sphere with radius $R_i + \overline{R}$ with spheres of size R_j. This is done by estimating the contact area between every two spheres to be $\pi \min(R_i^2, R_j^2)$. In this case, the choice of picking the minimum radius, leads to a symmetric contact area, meaning the contact area from grain i to grain j is the same as for grain j with grain i. This ensures the constancy of the overall volume of all spheres. Although [27] basic idea was to implement local neighbor variations, his model does not fully exclude $\overline{R}$ from his growth model, as can be seen on the left hand side of Eq. (3). Therefore in his model, the histogram of the coordination numbers, *i.e.* the probability distribution for the number of neighbors, does not fit to observed microstructures, because the mode is to small and the spread to narrow. His equation for grain growth yields :

$$\frac{dR_i}{dt} = -\frac{dR_j}{dt} \propto \gamma_{GB}\left(\frac{1}{R_j} - \frac{1}{R_i}\right) \tag{4}$$

Abbruzzese and Lücke [28,29] are also using Eq. (4) for the grain growth kinetic, but differ in the assignment of the neighborhood. Their approach is a statistical neighbor assignment instead of a discrete one. Therefore, they calculate the probability of grains with radius R_i to be neighboring a grain of radius R_j. Since this probability is symmetric, the probability of a grain i to be neighbor of grain j is the same as the probability of grain j to be adjacent to grain i, this approach intrinsically guarantees the overall grain area to be constant. While their approach is unimpeachable from a mathematical point of view, its implementation is kind of impractical. The probabilistic assignment of neighbors is based on an inherent probability function, that outputs the probability of a given grain, to be within size class r_i and having n neighbors. [28,29] obtained this function by fitting it to the data, extracted from the microstructure of a Al 3% Mg sample.

The model proposed here fits into this group of models that try to expand the basic models by incorporating microstructural features that arise from local inhomogeneities, without the necessity of a lateral resolution of the simulation itself, hereby bypassing the increased computation time that is characteristic for these models. Nevertheless, if results with a lateral resolution is desired, vertex or phase field models are still the way to go.

3. Experimental procedure

For the model validation, a CMn-steel (0.04 wt% C, 1.6 wt% Mn, 0.3 wt% Si, 0.03 wt% Al) has been analyzed during grain growth regarding its grain size kinetics and its characteristics concerning grain neighbor counts and grain neighbor size analysis. Equivalent grain diameters in a 2D cross section were determined in the initial state and for heat treatments at 1050 °C, 1150 °C and 1250 °C respectively for 10, 20, 45, 60, 120 and 240 min. Samples were cut open in the middle and the grain size was determined. To do so, a substantial amount of grains is necessary to confirm the reliability of the measured values and to prevent misinterpretation due to statistical insufficiency. Due to the limited scanning area and time, an EBSD reconstruction is therefore not the method of choice, especially when the microstructure has formed mainly diffusion controlled. A new procedure has been used that has been particularly developed to overcome this problem. It is based on deep learning algorithms and capable to analyze a couple thousands of grains within minutes from a Bechet–Beaujard etching, as described in [20]. It has been calibrated using reconstructed microstructure from EBSD data and has been extensively tested to provide reliable results.

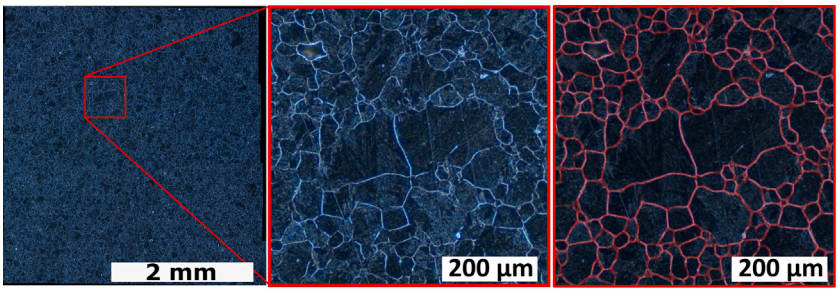

Fig. 1. Example of a panorama image of an etching. Grain boundaries have been extracted as described in [20] and shown on the right.

Grain size analysis and grain neighbor analysis haven been done using the Software Fiji and MatLab. To ensure a good agreement between simulated and present temperature profile within the sample, the exact temperature profile of the heating up phase was measured with a thermocouple in the core of a dummy specimen. An example of the etchings where grain size and the neighbor grain analysis have been performed is shown in Fig. 1 below.

4. The proposed model

4.1. Creating neighbor relations from grain size distribution

Although [27] never presented the distribution regarding the number of neighbors of the grains in his work, applying the algorithm given with Eq. (3) to the given grain size distribution of a given microstructure, the resulting distribution is too narrow in comparison. Considering that the method is intended for 3 dimensions, compared to a two dimensional cross section of a three dimensional structure, the neighbor distribution peak value at four seems to be too small. A distribution peak value of four to five can be observed in measurements of 2D cross sections, whereas the value in three dimension has to be higher, due to the additional neighboring grains in the missing third dimension. Therefore a similar but different procedure is presented that is independent of the assumptions of the contact area between grains, as used in Eq. (3). It also bypasses the correction value of $\overline{R}$, which could easily confound the results for bi- or multi modal size distributions, and also does not require the probability calculations and fits as in [28,29].

The principle of the new method is based on the idea, that at equilibrium conditions the angle at triple junctions of grains should be 120° in 2D and 109° at quadruple junctions in 3D for missorientation independent interfacial energies γ_{GB}. Assuming an extreme monomodal grain size distribution this results in six neighbors for each grain in the 2D case and in 12 for the 3D case. The 12 neighbors in three dimensions come from the sufficient similarity between the 109° equilibrium angle and the 108° angles of a dodecahedron which has 12 faces. In mathematical terms this breaking condition can be expressed in similar ways as Eq. (3), as:

for grain i: $$1 \leq \sum_{j=1}^{j_{max}} \frac{1}{6} \frac{R_i}{R_j} \quad \text{in 2D} \tag{5}$$

and

for grain i: $$1 \leq \sum_{j=1}^{j_{max}} \frac{1}{12} \frac{R_i}{R_j} \quad \text{in 3D} \tag{6}$$

The denominator values of 6 and 12 ensure, that a grain that is on average larger than its neighbors, has more neighbors then the denominator value and vice versa. This ensures, according to Eq. (9), the von Neumann–Mullins relationship, consequently in 2 dimensions grains with more than 6 neighbors (12 in 3 dimensions) grow and grains with less than 6 neighbors, respectively 12, shrink. Even though in reality the observations deviate in the individual cases, the overall grain growth behavior follows the von Neumann–Mullins relationship, even for anisotropic grain boundary energy, as shown by [30].

For fine tuning, the denominator values of the prefactors in Eqs. (5) and (6) can be slightly adapted until the generated distribution represents reality in the best possible way. A similar effect has been observed by [28], as he had to correct the grains perimeter compared to its radius. It is assumed that also in the case presented the reason is the same and can be traced back to not perfectly equiaxed grains, which results in a slight deviation from the spherical assumed shape of the grains. Applying the presented approach to a given grain size distribution, results in a coordination number distribution as shown in Fig. 2.

As displayed in Fig. 2, the neighbor assignment can start at any arbitrary grain. Starting at any index i, grain i is linked alternating to grains with higher and lower index, until the breaking condition in Eq. (5) occurs. If the index would become smaller than zero or larger than the number of radii, it attains the corresponding index value from the end of the array or at the start of the array. Visually, the array is virtually connected to its own end as pictured. This procedure is repeated for every grain, considering their already existing links from earlier treated grains, linked to them. Eqs. (5) and (6) are in fact inequations, since it can be assumed that there is no linear array of arbitrary grain radii R_i, that would result in Eqs. (5) and (6) being exactly 1. For this reason, the contact area between two grains, cannot be extracted from these equations, since those contact areas would be asymmetric, accordingly the conservation of area or volume during grain growth would be violated. Hence, a symmetric expression for the contact area a_{ij} is given in following Eqs. (7) and (8).

$$a_{ij} = \pi \frac{2}{6} \frac{R_i + R_j}{2} \quad \text{in 2D} \tag{7}$$

and

$$a_{ij} = \pi \frac{1}{9} \left(\frac{R_i + R_j}{2} \right)^2 \quad \text{in 3D} \tag{8}$$

These equations, which draw the grain boundary between grain i and grain j exactly in the middle at $\frac{R_i+R_j}{2}$, can be interpreted as the construction of a Voronoi cell, as depicted in Fig. 3.

4.2. Re-adjusting neighbors during grain growth

During grain growth it inevitably comes to the disappearance of grains, since they are absorbed by their neighbors. Consequently, the neighbors lose the vanished grain as their neighbor. For growing grains, this leads to the stage that no neighbors are left, and their ability to grow is reduced to zero. To avoid this, their grain boundary area has to be reoccupied. This reoccupation is conducted under the same rules as given in Eq. (5) or (6), with one exception. Only grains that also lost the exact same neighbor come into consideration for reoccupation and this method is applied for all grains that lost a neighbor. For simplicity, the reallocation is only done when a grain disappears and not after each discrete time step, even though Eq. (5) or (6) might not be satisfied in between anymore due to the change of size of individual grains. A disadvantage of this method is that time steps cannot have arbitrary values, but the values are limited to a value so that only one grain

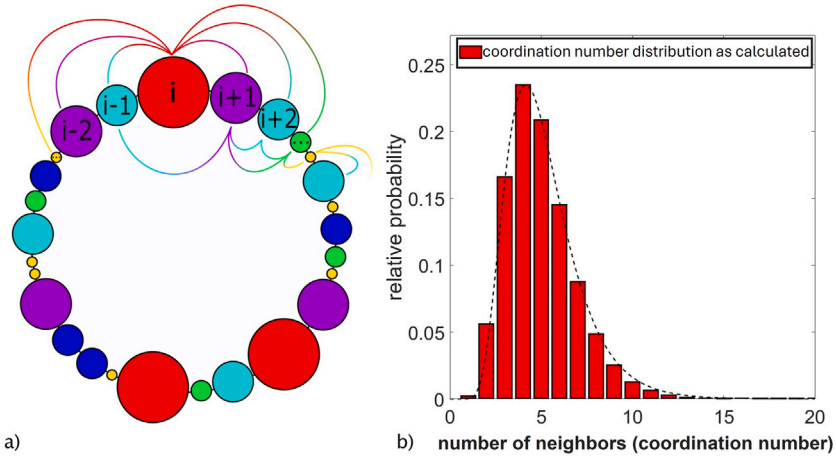

Fig. 2. (**a**) An array of grain radii in random order is generated so that their histogram represents the desired size distribution. Subsequent the grains are linked. (**b**) Corresponding coordination number distribution generated by Eq. (5) for 67.000 grains, with a log-normal distribution fitted to it.

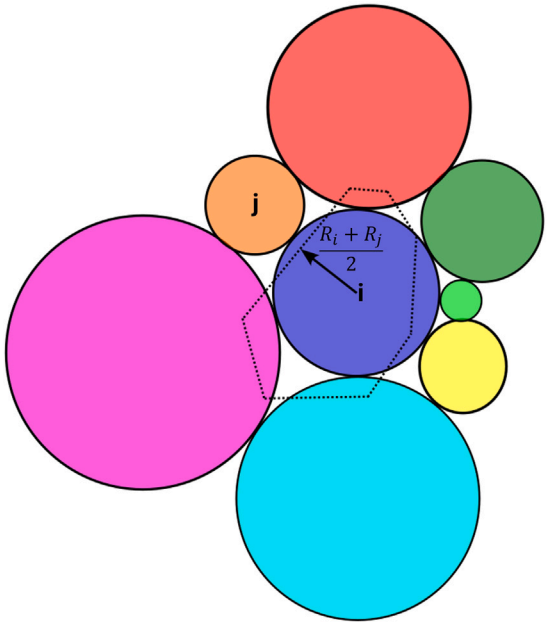

Fig. 3. Visualization of Eq. (7). Grain boundary segments of a polygon, constructed as a Voronoi cell.

among all will disappear in that particular time step. The reason behind is simply that after a grain disappears and the neighbors are reallocated, the individual driving forces (see Section 4.3) have to be reevaluated. If an individual time step might be too large so that the individual volume change for each grain indicates that more than one grain would vanish, this can be corrected by rescaling the time step so that only for one grain the negative volume change equals the grains area or volume. Thus the whole following procedure in Sections 4.3 to 4.4 does not have to be recalculated. This method can also be applied to refine the calculations in such a way that time steps limit the grains volume change per time step, so that they do not change their size over magnitudes in a single time step.

4.3. Evaluation of the driving force

The driving force in this work is still based on the thoughts of [4], but with respect to the generated neighbor relations in Section 4.1. It is composed of 2 terms, respectively for driving forces through boundary curvature and driving forces by dislocation density differences. The driving force of grain "i" with regard to its neighbor grain "j" can be expressed as:

$$F_{i\to j} = -F_{j\to i} = \gamma_{ij}\left(\frac{1}{d_j} - \frac{1}{d_i}\right) + 0.5Gb^2\left(\rho_j - \rho_i\right) \tag{9}$$

where γ_{ij} is the homogeneous, isotropic grain boundary energy, $d_{i,j}$ the diameter of grain i and j, G is the shear modulus, b the burgers vector and $\rho_{i,j}$ the dislocation density of grain i and j. If grains are of equal size, the force resulting through boundary curvature is zero. In cases where recrystallization occurs, hence deformation free small nuclei start growing at the expense of their surrounding deformed grains, the second term based on the dislocation density overwhelms the first one. The fact that $F_{i\to j} = -F_{j\to i}$ ensures the simulated volume to remain constant during grain growth, since the fluxes for the Eulerian control volume for each grain boundary add up to zero.

For all grains the calculations by Eq. (9) are independent and therefore can be parallelized. Because of the symmetry in the same equation, the quantity of calculation can be further reduced making this approach very efficient with respect to computation time.

4.4. Bypassing the limitation of maximum grain size to be about the simulation area or volume

In reality grains cannot grow larger than a monocrystal. The maximum grain size is thus limited by the available volume. Therefore it is necessary in the simulation as well, to provide enough total volume at the beginning to not confound the final grain size by to few initial grains. However, a large number of grains at simulation start also provokes disadvantages. Even thought the computation time per time step will diminish over time due to the decreasing number of grains, the total computation time will be drastically increased. To avoid this dissipation and at the same time bypass the maximum grain size problem described above, a new method is presented.

For better visualization, one can imagine observing grain growth in a limited area under a microscope. When the number of grains in this area is decreased in such a way, that it is impossible to calculate values as mean grain size etc. with high statistical certainty, one decreases the magnification and continues observing grain growth, but now with better statistics.

In reality this is simple, because after enlarging the field of view, it is obvious if the now statistical sufficient number of grains matches the expectations from the small area before or if the small area represented some outliers compared to its surrounding. In the simulation this is impossible because there are no grains outside the box. The newly created structure and its properties are entirely based on the previous

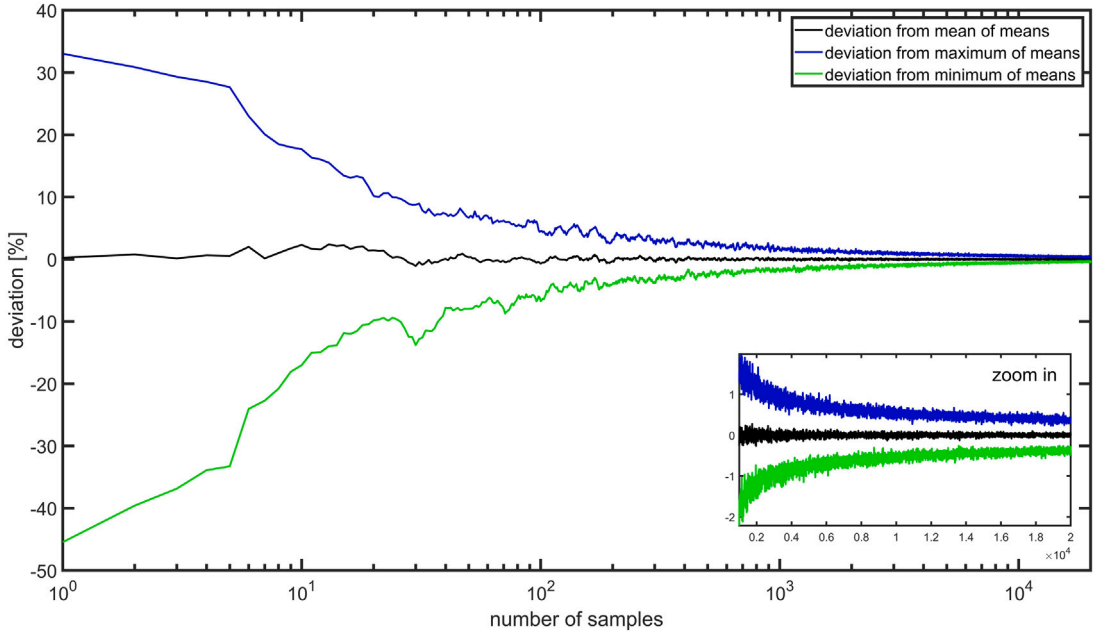

Fig. 4. For every integer value on the x-axis, x random numbers were taken 10 times, following the log-normal distribution with the parameters. $\mu = log(20)$ and $\sigma = log(1.4)$. For each of the 10 test series the mean value was calculated. On the y-axis the deviation from the expected value of the mean of those 10 mean values (black), the maximum of the mean values (blue) and the minimum of the means (green) is plotted. For the mean to have a maximum deviation of 1% from the expectation value $e^{\mu+\frac{\sigma^2}{2}}$, at least 2000 data points or more are necessary. Adding a security margin, 2500 samples are required.

structure. Thus the "zoom out" in the simulation has to happen before the number of grains is to few and the system becomes indescribable in a statistical manner. In Fig. 4 it is shown how the lower limit of necessary grains is statistically determined by a simple evaluation of statistics.

To increase the number of grains, the existing grains including their properties, except their neighbor relations, are copied and replicated. The replication factor can be any integer value greater than or equal to 2. The manifold grains are then attached in a special way to the existing grain array. One can imagine from Fig. 2 (a), that the circle is broken down, bend up and the gap is filled with an almost copy of its own. The modifications applied to the duplicated array are the following:

1. For each of the two grains bordering the insertion point, determine their neighbors on the opposite side of the insertion point.
2. Keep the grains from point 1. in this exact sequence, to not manipulate the neighbor relations of the existing grains at both ends of the insertion point.
3. Mix the remaining grains in a random order and allocate neighbors to them according to Eqs. (5) or (6). The mixing has to be done, since otherwise the copied grains would have allocated the corresponding neighbors of the original array. This would result in an amplification of the characteristics of the grain size distribution that might not be beneficial.

A schematic example of this procedure is illustrated in Fig. 5:

5. Results and discussion

The calculated neighbor histogram matches the measured neighbor histogram very well for only being based in the 120° equilibrium angle assumption, as can be seen in Fig. 6.

The artificial microstructure can be further analyzed to compare it with properties of the real microstructure. Therefore, both the artificial as well as the real microstructure were examined for grain-neighbor grain properties. In detail, the correlation between the grain size and the number of neighboring grains (coordination number) was evaluated (Fig. 7), as well as the correlation between the grain size and the size of the neighboring grains (Fig. 8).

While the shapes of both probability distributions in Fig. 7 are similar, they have minor differences. The width of the artificial distribution (middle) seems a bit wider than its counter part (top). Related to Fig. 6 and its deviations it can be concluded that those deviations can only result from the deviation of a spherical grain shape in the measured microstructure, whereas a spherical shaped grain in the model is assumed. On the other hand, the relative size of the neighbor grains (Fig. 8) seems unaffected by this. Compared with the microstructural data from an Al 3% Mg sample provided by [28], the data from the sample in this work as well as from the artificial microstructure show a very good agreement. In all cases the spread of the distribution is in conformity. Fig. 7 (bottom) confirms this, where only minor deviations of the linear regression from real and artificial microstructures are visible. The largest difference can be observed when comparing the data to the coordination number calculated by $n = 3 + 3\overline{R}$. While this theoretical approach is also based on the assumption of 6 neighbors for equally sized grains, it also assumes a minimum neighbor count of 3 in 2-dimensions. This is in contradiction to the real microstructure which shows as little as 2 neighbors on a regular basis, which is also the case for the artificial microstructure proposed in this paper

Parameters in Table 1 were chosen to give the best overall agreement for the values of maximum grain size, area weighted mean grain size, number weighted mean grain size and the 95% percentile of all grains and for all times and temperatures as can be seen in Fig. 9.

The influence of the artificial microstructure on the grain growth behavior itself has been also put to the test. Fig. 10 shows a comparison between experimental results for a CMn-steel and 4 nearly identical simulations. All 4 simulations have the exact same grain size distribution as starting condition in common, but since the order is different, they differ in the assignment of the neighbor relations of the individual grains. As can be seen, the tendency of all 4 simulations is the same. The 5 properties displayed, namely minimum grain diameter, number weighted mean grain diameter, area weighted mean grain diameter, 95% percentile and maximum grain diameter, all have about the same values with a good agreement of the measured values. The spread of

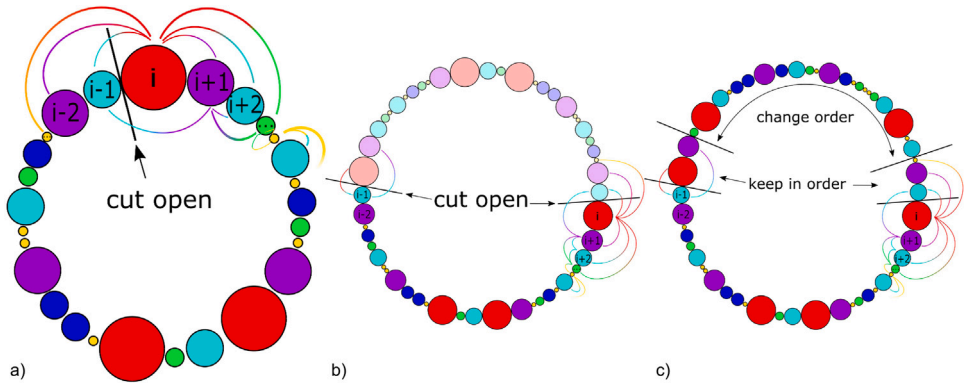

Fig. 5. (**a**) Cut the grain array from Fig. 2 (a) open at any arbitrary position. Count to how many grains the grains at one cut side are connected to grains of the other cut side (red grain (i) is connected to 3 to grains to the left, turquoise grain ($i-1$) is connected to 2 grains to the right) (**b**) insert a copy of the array into the cutting point (**c**) keep the 3 new neighbors to the left of the red grain (i) and accordingly the 2 new neighbors to the right of turquoise grain ($i-1$) in the exact sequence while the order of the grains between is mixed up. Subsequently assign neighbors to the new grains according Eq. (5) or (6).

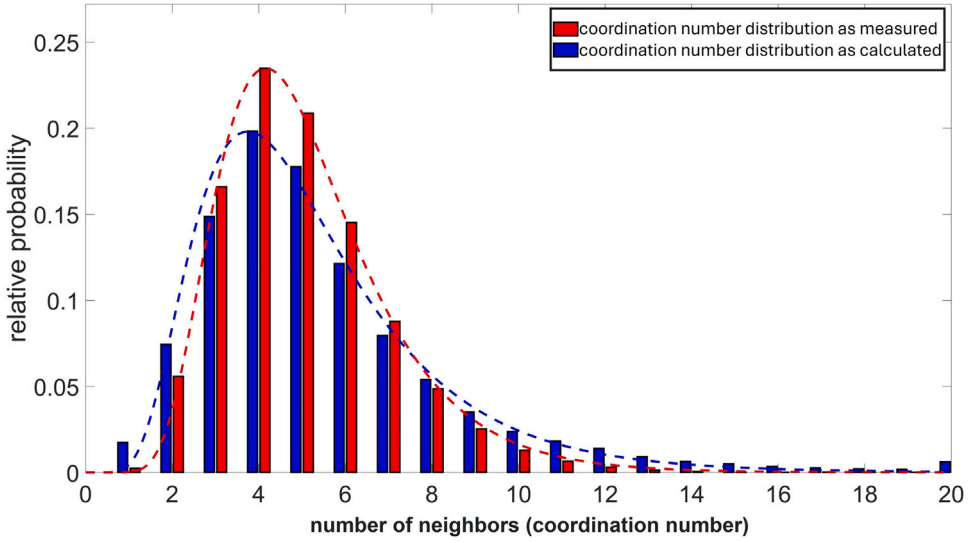

Fig. 6. Comparison between measured (blue) coordination number distribution and calculated (red) coordination number distribution. Both are characterized by a maximum number of neighbors of 20 and a peak value at 4. The slight left shift of the measured distribution compared to the calculated one, is argued to come from the assumption of spherical grains, which seems to be not fully applicable. The blue histogram is based on 67 000 grains, measured by EBSD, the red one is also based on 67 000 grains, following the same size distribution as measured.

Table 1
Input parameters for grain growth simulation.

Parameter	Value	Source
γ	1.3111-0.0005T	[31]
G	$\frac{E}{2(1+\nu)}$	general knowledge
ν	0.3	this work
E	(191000-73T)·10^6	this work
b	360·10^{-12}	this work
Fine tuned denominator value Eq. (5)	5.5	this work

Table 2
Mean values (A.M.) and standard deviations (SD) after 4 h at 1250 °C of plotted properties in Fig. 10 based on 10 simulations.

Property	A.M. [μm]	SD [μm]	$\frac{SD}{A.M.}$ [%]
Maximum grain size	3,461.3	519.9	15.0
95% of grains below	1,321.7	107.6	8.1
Area weighted mean grain size	1,055.6	91.9	8.7
Number weighted mean grain size	779.1	33.1	4.3
Minimum grain size	150.7	23.7	15.7

these values displayed and evaluated in Table 2 is expected to be the same for 4 individual samples that have been heat treated under the same conditions.

Comparing simulations where the "zoom out" method proposed from Section 4.4 was applied and simulations where it was not applied (Fig. 11), show a close match up to a distinctive point.

Both progressions in Fig. 11 are nearly identical beyond the point where the conventional method drops below 2500 grains, showing that the new method does not influence the results. Noteworthy diverging between both simulations starts between the "500 grains" mark and "200 grains" mark, which flag the points where the conventional method drops below 500, respectively 200 grains. Even though the diverging itself could be of statistical nature, due to too few grains, it is also fact that with too few grains the chances for every grain to satisfy Eq. (5) during neighbor reallocation is reduced. This leads to a wrong neighbor distribution which also influences further performance. In summary, the new method presents a favorable alternative since the results are less influenced by the individual behavior of single grains, if the number of grains is statistically insufficient (kinks in dashed lines). The major advantage remains in the reduction of computation time

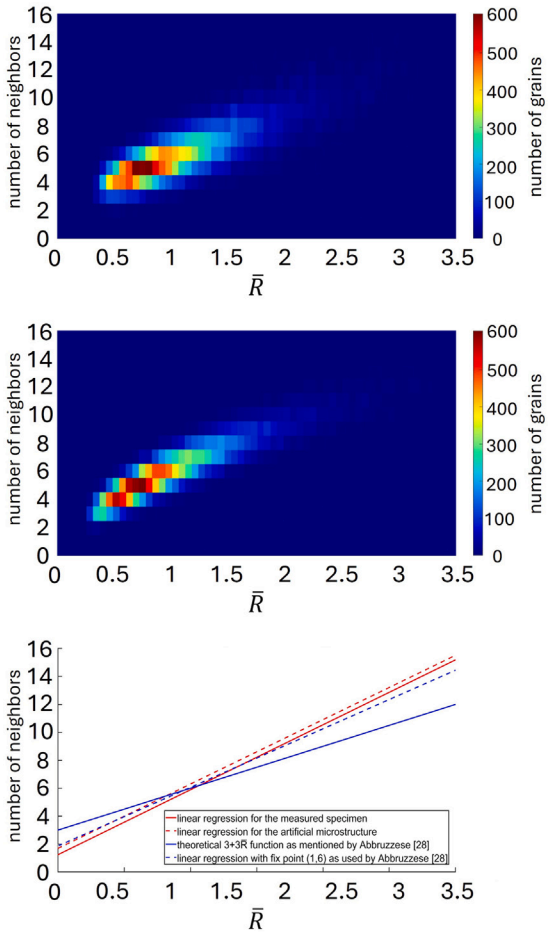

Fig. 7. Comparison between the correlation of the normalized grain size regarding $\bar{R}$ and its number of neighbors for the measured specimen (top) and the calculated artificial microstructure (middle). Comparison is also possible with respect to the fit function used by [28] (bottom).

which has been reduced by 97% from about 8.61 h to 13 min, for the simulation of 1 h grain growth at 1250 °C including the heating-up.

To underline [32], in which the state is independent on initial conditions, this can be put to the test by simulating the same heat treatment but with different initial grain size distributions. Three distributions have been chosen which not only differ in parameters of the distribution but in the distribution itself, namely a left skewed log.-normal distribution, right skewed log.-normal distribution and a Gaussian distribution. It can be seen in Fig. 12 that independent on the initial distribution, within the relative deviations of the grain sizes illustrated in Fig. 10 and Table 2, the results remain the same. In the zoomed in version, Fig. 12 (c), this converging point can be found very early after only about 6 min, which is before the final temperature has been reached at 6:40 min.

Looking at 13, it is evident that the grain size distributions is widening with time (see Fig. 13). [3] published data that are very similar and also support this behavior. A general observation is, that even if the maximum grain size relative to the mean grain size is very large at the start, it drops almost immediately to a value of about 2, which is the maximum value according to [3] observed for normal grain growth. The fact that, in agreement with the measurements, after this drop the ratio starts to increase again up to a steady state value of about 3.5 to 4 for all temperatures, suggests that all samples undergo some kind of abnormal grain growth and that this behavior is already covered by the simulation. While it is very hard to backtrack this manner, it is assumed that it must come from special configurations of the neighborhood relationship of individual grains.

By manipulating the rather random order of the grains size array before the neighbor relations are allocated, their sequence can be influenced and the effect on grain growth can be observed. For example an humongous grain surrounded by tiny grains, compared to the same enormous grain surrounded by average sized grains could be analyzed for the impact of the neighbor configuration on the grain growth kinetics. Considering strain induced grain growth and recrystallization this dependency gains in significance. Questions such as if some giant grains, arisen by coarsening, can totally change a recrystallization kinetic or if this would additionally depend on their neighbors can be answered. For such purposes the here proposed method is ideal if a more complex model with lateral resolution is too time consuming.

5.1. Possible expansions to include texture evolution

The model expansion discussed hereinafter is not included yet, but would be easy to implement and favor from the structure of the general approach:

In 4.3, the interfacial energy is taken as a temperature dependent value, independent of the grain neighborship. In reality γ is depending on the missorientation of the grains and the exact geometry of the grain boundary, such as the normal vectors of the grain boundaries. While the grain boundary geometry is not included by the presented approach, assigning each grain an orientation, the missorientation between neighboring grains can be calculated and also the dependency of γ on the same. The calculation of the interfacial energy is taken from [33]. Since the iterative evaluation would be too time consuming, the orientation space is discretized and these discrete orientations are randomly assigned to the grains. The precalculated missorientation concerning the grains orientations and the corresponding γ-values are taken from look up tables. The mobility of the grain boundary is dependent on the missorientation θ and calculated by

$$M(\theta) = M_0 \cdot \left[1 - exp\left(-5\left(\frac{\theta}{\theta_0}\right)^4\right)\right] \tag{10}$$

according to [34], with $\theta_0 = 15°$ being the threshold missorientation with a constant, misorientation independent mobility above it.

The grain boundary mobility M_0 is directly taken from the mobility values provided by the CALPHAD approach. These values can be further corrected for solute drag and Zener pinning, presented in [35].

During deformation and recrystallization the texture, hence the individual orientations of the grains will change. The path in orientation space that each orientation will take during deformation can be calculated by either Taylor- or Sachs model. Since these orientation changes require the orientation space to be discretized very fine, it is advised to interpolate the misorientation and interfacial energies between those states, otherwise the fine discretization, resulting in a number of precalculated misorientations proportional to the square of the discrete orientations, would be very hungry for system resources.

New grains forming during recrystallization could be initialized with a random orientation that has a low interfacial energy towards its neighbor grains.

6. Conclusion

In this work, an algorithm to link individual grains to generate an artificial microstructure with discrete neighbors is presented. The approach is based on the observations of dihedral angles of 120° in structures with isotropic interfacial energy. Its independent of assumptions about the contact area between grains and bypasses the problems of older ideas that were dependent on informations extracted from real microstructures. Based on that, multiple examinations within the simulation can be investigated, that cannot be studied with other purely statistical grain growth models:

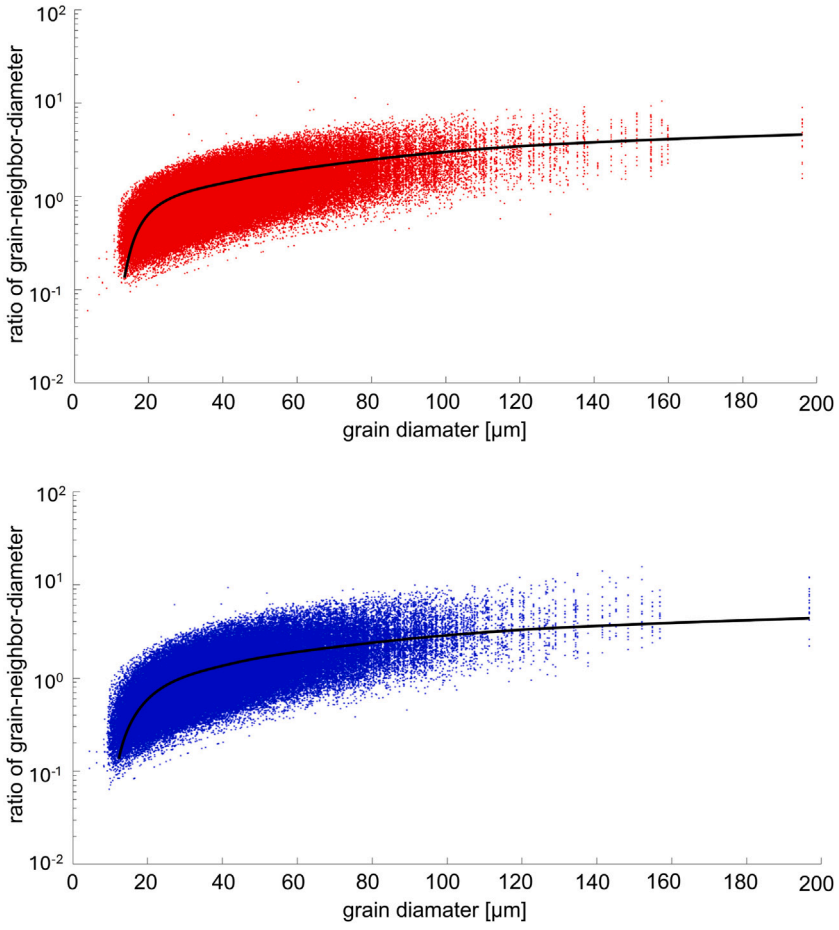

Fig. 8. Comparison between the correlation of grain size and the size of its neighbor grains for the measured specimen (top) and the calculated artificial microstructure (bottom).

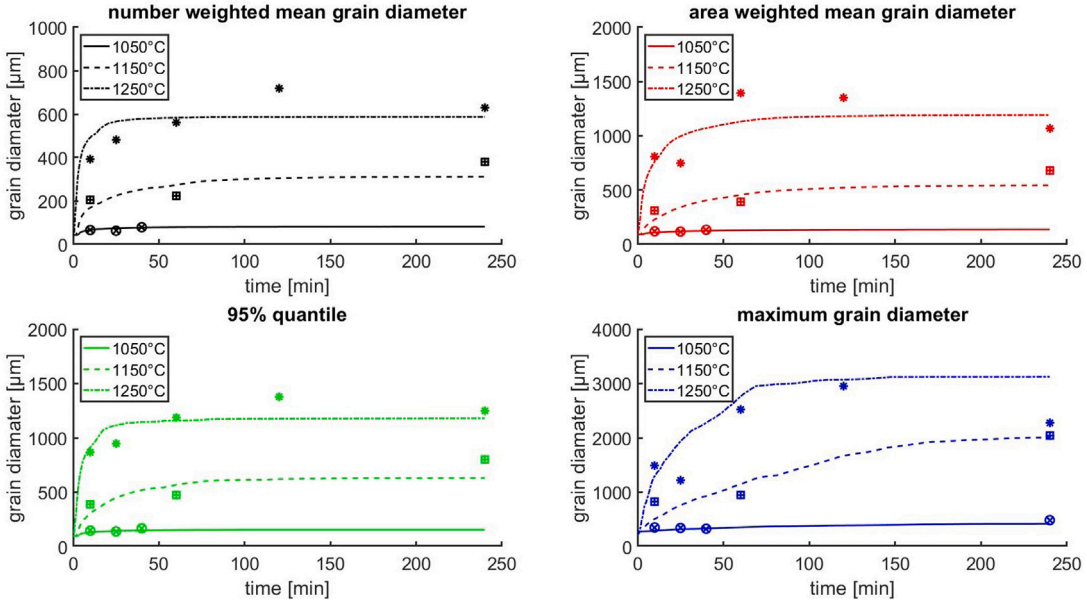

Fig. 9. Temperature dependent grain growth: Comparison between simulation and measurements. Measured data points are marked with ⊗ for 1050 °C, ⊞ for 1150 °C and ∗ for 1250 °C , whereas the simulation results are plotted in solid, dashed and dotted lines for the different temperatures. Missing datapoints are owed to the fact that from some samples no grain size could be extracted, due to bad etching quality, mainly caused by bainitic dominated microstructures.

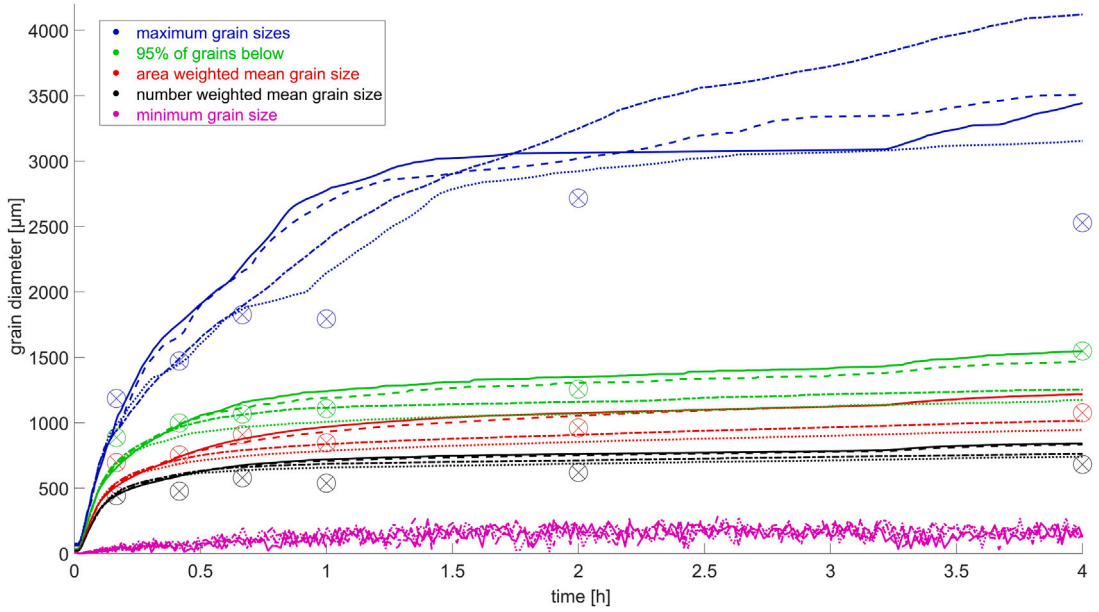

Fig. 10. Comparison between measured values (marked with ⊗) and corresponding simulated values for 4 simulations of a CMn- steel at 1250 °C. It can be observed that the different profiles of the 5 properties plotted all have the same tendency and order of magnitude (see Table 2).

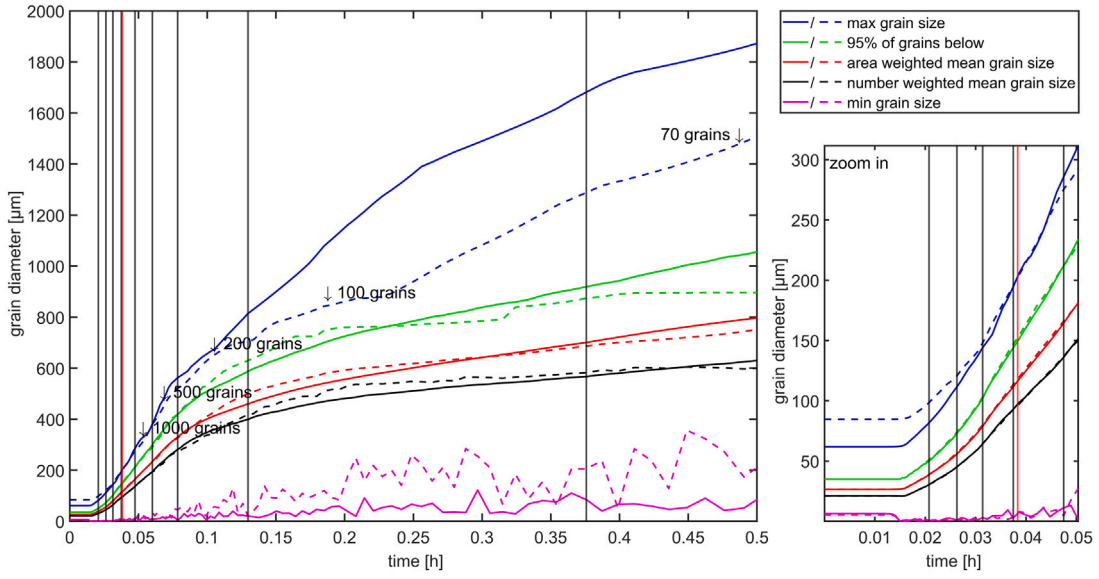

Fig. 11. Comparison between the new method (continuous lines) and a conventional method (dashed lines). The simulation with the new method started with 5000 grains, using the "zoom out" function when the grain number would drop below 2500 grains, marked with black vertical lines. The Conventional simulation started with 40 000 grains. The vertical red line marks the time where the conventional simulation drops below 2500 grains.

- The model is able to reflect morphological aspects of a real microstructure. This includes:
  - the dependency of the coordination number distribution of the grain size distribution
  - the dependency of the coordination number of the grain size
  - the dependency of the grain size on the size of the neighboring grains
- For microstructures that are statistically identical regarding its grain size, the influence of the individual grain neighbor on the coarsening behavior can be observed. In the case of a random linking, it can be shown that different linkings result in a slight scatter in the grain size over time, as one would expect it to be for different samples that went through the same heat treatment. The amount of scatter within grain size development over time can therefore be investigated.
- The initial grain size distribution affects the grain neighbor size correlation. It can be shown that the grain size distribution always evolves into a log-normal distribution, unaffected by the initial grain size distribution.
- To continue the thought of point 3, it is possible to investigate how different nucleation sites during nucleation, either nucleation at smaller grains or larger grains, can affect the recrystallization kinetics and the grain size distribution after recrystallization.

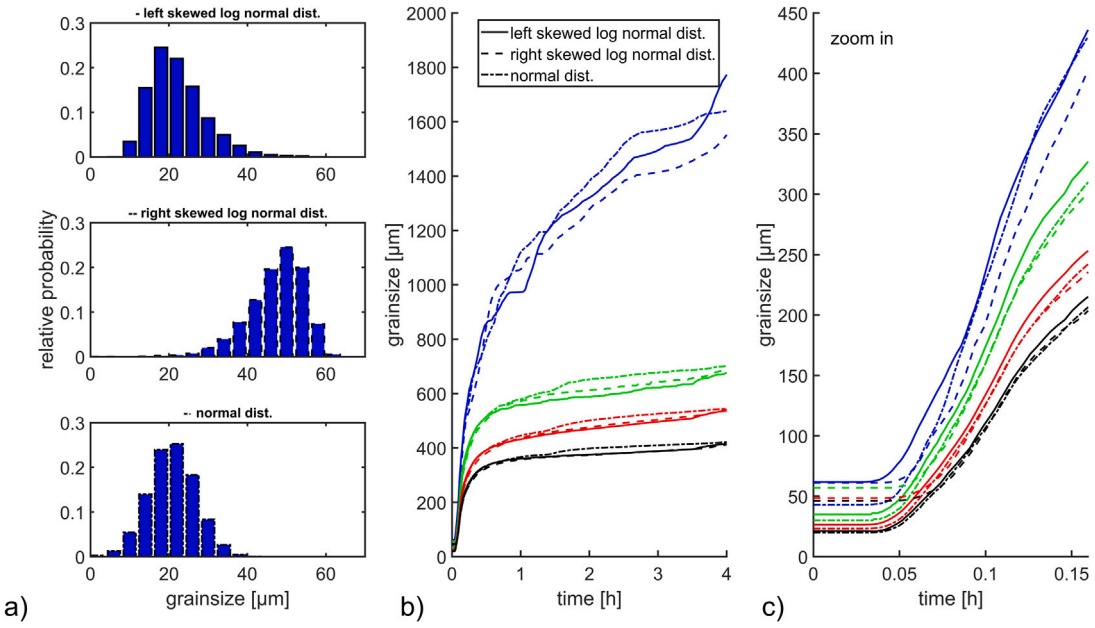

Fig. 12. Grain growth independent on initial state. Colors assignment identical to previous Figures: blue for maximum grain diameter, green for 95% quantile, red for area weighted mean grain diameter and black for number weighted mean grain diameter **(a)** different initial grain size distributions **(b)** grain growth over time at 1150 °C for 4 h **(c)** zoomed in version of first 10 min of **(b)** with visible heating-up section at the beginning.

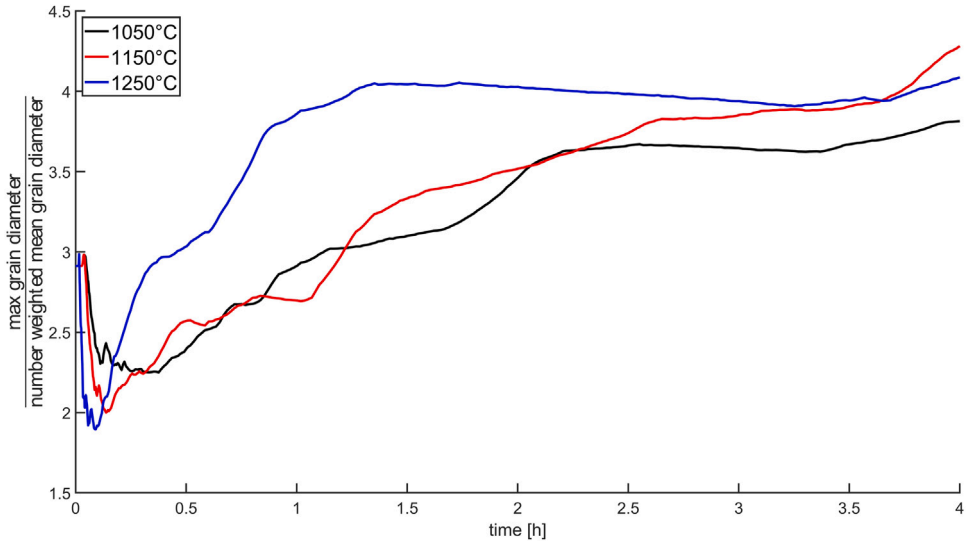

Fig. 13. Analysis of the widening of the grain size distribution with time. The increase in ratio of the maximum grain size in relation to the mean grain size indicates that the largest grains grow faster than the average.

CRediT authorship contribution statement

Marc Laub: Writing – review & editing, Writing – original draft, Validation, Software, Methodology, Investigation, Conceptualization. **Eric Detemple:** Writing – review & editing. **Sebastian Scholl:** Writing – review & editing. **Christian Motz:** Writing – review & editing, Project administration.

Declaration of competing interest

The authors declare that they have no known competing financial interests or personal relationships that could have appeared to influence the work reported in this paper.

References

[1] P.A. Beck, Annealing of cold worked metals, Adv. Phys. 3 (11) (1954) 245–324, http://dx.doi.org/10.1080/00018735400101203.

[2] P. Feltham, Grain growth in metals, Acta Metall. 5 (2) (1957) 97–105, http://dx.doi.org/10.1016/0001-6160(57)90136-0.

[3] M. Hillert, On the theory of normal and abnormal grain growth, Acta Metall. 13 (3) (1965) 227–238, http://dx.doi.org/10.1016/0001-6160(65)90200-2.

[4] J.E. Burke, Some factors affecting the rate of grain growth in metals, Aime Trans. 180 (1949) 73–91.

[5] J.A. Ewing, W. Rosenhain, Viii. the crystalline structure of metals.(second paper), Philos. Trans. R. Soc. Lond. Ser. A, Contain. Pap. A Math. Phys. Character 195 (262–273) (1900) 279–301.

[6] R. Vogel, Über den wechselseitigen auf-und abbau sich berührender metallischer kristallite im konglomerat, Z. Anorg. Allg. Chem. 126 (1) (1923) 1–38.

[7] G. Tammann, Über die änderung der eigenschaften bei der bearbeitung von metallen, Z. Elektrochem. Angew. Phys. Chem. 18 (14) (1912) 584–601.

[8] C.E. Krill LII, L.Q. Chen, Computer simulation of 3-d grain growth using a phase-field model, Acta Mater. 50 (12) (2002) 3059–3075, http://dx.doi.org/10.1016/S1359-6454(02)00084-8.
[9] D. Raabe, Introduction of a scalable three-dimensional cellular automaton with a probabilistic switching rule for the discrete mesoscale simulation of recrystallization phenomena, Phil. Mag. A 79 (10) (1999) 2339–2358, http://dx.doi.org/10.1080/01418619908214288.
[10] M.P. Anderson, D.J. Srolovitz, G.S. Grest, P.S. Sahni, Computer simulation of grain growth—I. Kinetics, Acta Metall. 32 (5) (1984) 783–791, http://dx.doi.org/10.1016/0001-6160(84)90151-2.
[11] D.J. Srolovitz, M.P. Anderson, P.S. Sahni, G.S. Grest, Computer simulation of grain growth—II. Grain size distribution, topology, and local dynamics, Acta Metall. 32 (5) (1984) 793–802, http://dx.doi.org/10.1016/0001-6160(84)90152-4.
[12] K. Kawasaki, T. Nagai, K. Nakashima, Vertex models for two-dimensional grain growth, Phil. Mag. B 60 (3) (1989) 399–421, http://dx.doi.org/10.1080/13642818908205916.
[13] E.A. Lazar, R.D. MacPherson, D.J. Srolovitz, A more accurate two-dimensional grain growth algorithm, Acta Mater. 58 (2) (2010) 364–372, http://dx.doi.org/10.1016/j.actamat.2009.09.008.
[14] L.S. Shvindlerman, G. Gottstein, A.D. Rollett, The Von Neumann-Mullins theory of grain growth–Valid or not?! in: Materials Science Forum, Vol. 467, Trans Tech Publ, 2004, pp. 1111–1116, http://dx.doi.org/10.4028/www.scientific.net/MSF.467-470.1111.
[15] E.A. Lazar, J.K. Mason, R.D. MacPherson, D.J. Srolovitz, A more accurate three-dimensional grain growth algorithm, Acta Mater. 59 (17) (2011) 6837–6847, http://dx.doi.org/10.1016/j.actamat.2011.07.052.
[16] E.A. Lazar, J.K. Mason, R.D. MacPherson, D.J. Srolovitz, Corrigendum to: A more accurate three-dimensional grain growth algorithm [Acta Mater. 59 (2011) 6837-6847], Acta Mater. 71 (2014) 390, http://dx.doi.org/10.1016/j.actamat.2014.02.025.
[17] M. Maalekian, R. Radis, M. Militzer, A. Moreau, W.J. Poole, In situ measurement and modelling of austenite grain growth in a ti/nb microalloyed steel, Acta Mater. 60 (3) (2012) 1015–1026, http://dx.doi.org/10.1016/j.actamat.2011.11.016.
[18] L. Germain, N. Gey, R. Mercier, P. Blaineau, M. Humbert, An advanced approach to reconstructing parent orientation maps in the case of approximate orientation relations: Application to steels, Acta Mater. 60 (11) (2012) 4551–4562, http://dx.doi.org/10.1016/j.actamat.2012.04.034.
[19] S. Béchet, L. Beaujard, Nouveau réactif pour la mise en évidence micrographique du grain austénitique des aciers trempés ou trempés-revenus, Rev. Métallurgie 52 (10) (1955) 830–836.
[20] M. Laub, B.-I. Bachmann, E. Detemple, F. Scherff, T. Staudt, M. Müller, D. Britz, F. Mücklich, C. Motz, Determination of grain size distribution of prior austenite grains through a combination of a modified contrasting method and machine learning, Pr. Met. 60 (1) (2022) 4–36.
[21] G. Vander Voort, Wetting agents in metallography, Mater. Charact. 35 (2) (1995) 135–137, http://dx.doi.org/10.1016/1044-5803(95)80111-1.
[22] R. Thackray, E.J. Palmiere, O. Khalid, Novel etching technique for delineation of prior-austenite grain boundaries in low, medium and high carbon steels, Materials 13 (15) (2020) 3296, http://dx.doi.org/10.3390/ma13153296.
[23] D. San Martín, Y. Palizdar, R.C. Cochrane, R. Brydson, A.J. Scott, Application of nomarski differential interference contrast microscopy to highlight the prior austenite grain boundaries revealed by thermal etching, Mater. Charact. 61 (5) (2010) 584–588, http://dx.doi.org/10.1016/j.matchar.2010.03.001.
[24] J. Burke, D. Turnbull, Recrystallization and grain growth, Prog. Met. Phys. 3 (1952) 220–292.
[25] J. Von Neumann, Metal Interfaces, vol. 108, American Society for Metals, Cleveland, 1952, pp. 108–110.
[26] W.W. Mullins, Two-dimensional motion of idealized grain boundaries, J. Appl. Phys. 27 (8) (1956) 900–904, http://dx.doi.org/10.1063/1.1722511.
[27] O. Hunderi, N. Ryum, H. Westengen, Computer simulation of grain growth, Acta Metall. 27 (2) (1979) 161–165, http://dx.doi.org/10.1016/0001-6160(79)90091-9.
[28] G. Abbruzzese, I. Heckelmann, K. Lücke, Statistical theory of two-dimensional grain growth—I. The topological foundation, Acta Met. Mater. 40 (3) (1992) 519–532, http://dx.doi.org/10.1016/0956-7151(92)90401-Y.
[29] K. Lücke, I. Heckelmann, G. Abbruzzese, Statistical theory of two-dimensional grain growth—II. Kinetics of grain growth, Acta Met. Mater. 40 (3) (1992) 533–542, http://dx.doi.org/10.1016/0956-7151(92)90402-Z.
[30] M. Palmer, V. Fradkov, M. Glicksman, K. Rajan, Experimental assessment of the mullins-von neumann grain growth law, Scr. Met. Mater. 30 (5) (1994) 633–637.
[31] H.S. Zurob, C.R. Hutchinson, Y. Brechet, G. Purdy, Modeling recrystallization of microalloyed austenite: effect of coupling recovery, precipitation and recrystallization, Acta Mater. 50 (12) (2002) 3077–3094, http://dx.doi.org/10.1016/S1359-6454(02)00097-6.
[32] W.W. Mullins, The statistical self-similarity hypothesis in grain growth and particle coarsening, J. Appl. Phys. 59 (4) (1986) 1341–1349, http://dx.doi.org/10.1063/1.336528.
[33] V.V. Bulatov, B.W. Reed, M. Kumar, Grain boundary energy function for fcc metals, Acta Mater. 65 (2014) 161–175.
[34] E. Miyoshi, T. Takaki, S. Sakane, M. Ohno, Y. Shibuta, T. Aoki, Large-scale phase-field study of anisotropic grain growth: Effects of misorientation-dependent grain boundary energy and mobility, Comput. Mater. Sci. 186 (2021) 109992.
[35] H. Buken, E. Kozeschnik, Modeling static recrystallization in Al-Mg alloys, Met. Mater. Trans. A (2020) 1–9, http://dx.doi.org/10.1007/s11661-020-06100-9.